We are IntechOpen, the world's leading publisher of Open Access books Built by scientists, for scientists

4,800
Open access books available

122,000
International authors and editors

135M
Downloads

Our authors are among the

154
Countries delivered to

TOP 1%
most cited scientists

12.2%
Contributors from top 500 universities

CLARIVATE ANALYTICS BOOK CITATION INDEX INDEXED

WEB OF SCIENCE™

Selection of our books indexed in the Book Citation Index in Web of Science™ Core Collection (BKCI)

Interested in publishing with us?
Contact book.department@intechopen.com

Numbers displayed above are based on latest data collected.
For more information visit www.intechopen.com

5

Quasi–Nondiffractive Beams for OCT–Visualization: Theoretical and Experimental Investigations

Larisa Kramoreva, Elena Petrova and Julia Razhko
Gomel State Medical University, Gomel State Technical University, Republican Research Center for Radiation Medicine and Human Ecology, Gomel, Belarus

1. Introduction

Optical coherence tomography (OCT) is a method for imaging the internal structure of biological tissue *in vivo* with micron resolution. OCT has been recognized as an extremely promising tool for the diagnosis of pathological changes in biological tissue (Chauhan et al., 2001; Fercher et al., 2003). The coherence–domain range in OCT is performed by using a Michelson interferometer. By measuring singly back scattered light as a function of depth, OCT has the potential to image the structure of tissue with a high resolution and sensitivity. It is of importance for a diagnostics of structures inside a cornea, a cornea edema, for a quantitative imaging of the optic disc in glaucoma, for an evaluation of retinal thickness, etc. in ophthalmology. The high axial resolution of OCT is realized by the use of a broadband light source whereas the lateral resolution is determined by the numerical aperture (NA) of the focusing lens. Although a high NA of a conventional focusing lens in the sample arm of the imaging optical system enables high lateral resolution imaging, but low axial resolution. A low NA is required to achieve a large depth of focus, but in this case we deal with the low lateral resolution. The improvement of the axial–lateral resolution is a very important problem in imaging OCT-systems. Furthermore, a restriction of an imaging method is closely connected with a problem of tissue light–scattering: it leads to the decreasing in the focal depth of a probing beam and an image involves a "noisy"–speckle field superimposed on imaged structures as a result of scattering by a volume medium.

The impairment of optical mediums transparency, for example corneal caligo, opacity of vitreous body, cataract, causes the significant light scattering in the sample arm of OCT. In the case, when different pathologies in the macular area or in the optic nerve area occur the OCT–method doesn't give us a possibility to determine the reason of partial or complete sight loss. Fig. 1 demonstrates the non–informative OCT–image of retina for a patient with the cataract diagnosis (Fig. 1, a). After the surgical removal of opaque lens the retinal detachment was detected by the OCT–retest (Fig. 1, b). Before the surgical removal of the lens the retinal detachment was not detected by other methods, even the method of direct opthtalmoscopy. Fig. 1, c, d shows the OCT– image of the optic nerve area in a normal state (Fig. 1, c) and when we deal with the destruction in the vitreous body (Fig. 1, d). Thus

clinical investigations (Fig. 1, a–d) indicate the impossibility of correct image registration under the condition of strong tissue scattering (Kramoreva & Rozhko, 2010).

A scattering problem in OCT has been solved by numerical analysis of OCT–images. A possibility to estimate scattering properties of tissue layers by the dependence of OCT signal on a probing depth was demonstrated in several publications (Andersen et al, 2004; Schmitt & Knuttel, 1993; Turchin et al., 2003). In the majority of papers, the theoretical models of OCT signal that are employed in reconstruction algorithms use two optical parameters to describe the scattering medium: the total scattering coefficient and the backscattering coefficient (Schmitt & Knuttel, 1993; Turchin et al., 2003) or the total scattering coefficient and mean cosine of scattering angle. In other case the reconstruction algorithm allows one to estimate three scattering parameters, namely, the total scattering coefficient, the backscattering probability, and the variance of the small-angle scattering phase function. The reconstruction procedure for scattering parameters in a multilayer medium has a poor accuracy with the decrease in the thickness of a single layer (Andersen et al, 2004).

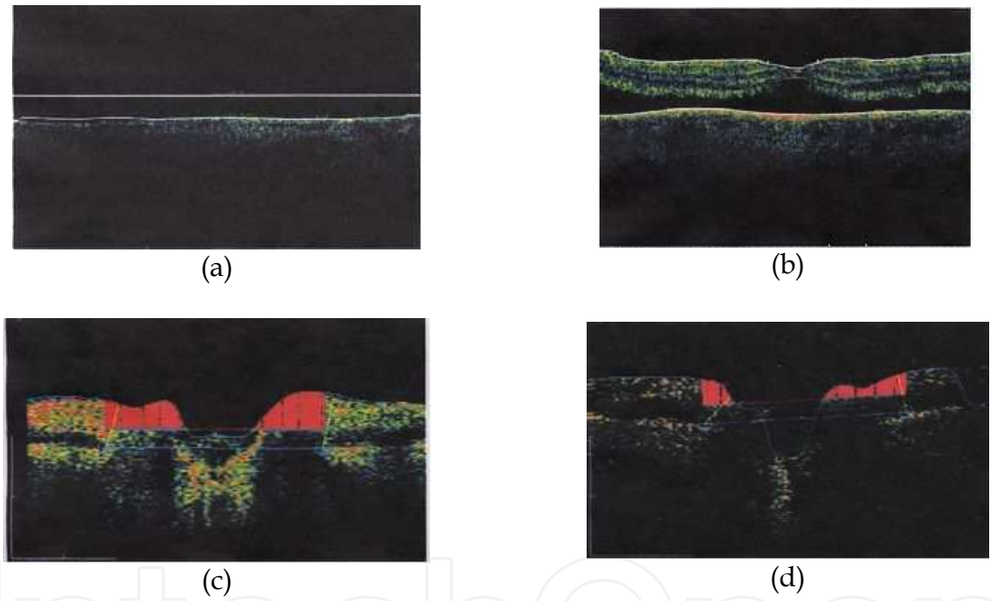

Fig. 1. The OCT – images of the macular area before (a) and after (b) the surgical removal of the opaque lens and the OCT – images of the optic nerve area in a normal state (c) and with the destruction in the vitreous body (d).

Therefore it is very important to improve the reconstruction algorithm of the OCT–signal. However, the contemporary design of optical elements is capable to improve the system resolution and image quality even before the final stage of computer processing.

From the viewpoint of foresaid the growing interest to various types of quasi-nondiffractive light beams (for example, a Bessel beam) is caused by the availability of unique properties: the large focal length of the beam, the suppressed diffraction divergence of the central part of the beam inside the focal length, the reconstruction of the transversal structure of the beam at the shielding of its central zone and a submicron structure of the axial maximum (for a nonparaxial and evanescent Bessel beam). These properties are promising for practical

applications requiring the laser beam with a large focal depth, including the interferometry of cylindrical objects (Belyi, et al., 2005; Dresel, et al., 1995), the coherent microscopy (Leitgeh et al, 2006),the optical manipulation of microparticles (Arit, et al., 2001; Garces–Chavez et al., 2002), etc. Together with advantages referred above Bessel beams have several drawbacks due to the feature of shaping units (Kramoreva & Rozhko, 2010). It reduces Bessel beam's efficiency in OCT–optical schemes. On the one hand, the development of new methods of the Bessel beam's generation with improved properties of the beam is a shortcut to an upgrading of the OCT–image problem.

On the other hand the electro–magnetic radiation absorption and the influence of tissue optical activity and scattering are the main optical effects under the condition of tissue probing.

Therefore, the knowledge about the objective laws of reflection and refraction for the probing radiation at the medium boundary is a necessary condition for high-quality diagnostics, for example, in the field of the polarizing sensitive tomography.

2. Generation of broadband Bessel-like beams: theory and experiment

The quasi-nondiffractive beam with the transverse intensity profile approximately corresponding to the zero-order Bessel function may be experimentally realized in the manner, which provides the annular-field generation in the far-field zone of the optical scheme. Traditionally simple ways of generation of the zero-order Bessel beam include the use of the annular ring mask placed at the front focal plane of the lens; the use of the refractive linear and logarithmic axicons illuminated by the collimated laser beam or the computer–generated axicon–type hologram (McGloin & Dholakia, 2005). However, for a probing Bessel beam, such disadvantages as the low energy-conversion efficiency, the nonuniform axial intensity (the residual sharp oscillation around the average intensity) within a focal length of a beam or the nonuniform of the central–core width of focal segment of the beam (Burval, 2004), can lead to a degradation of the image quality in different optical schemes including OCT.

In this section we consider the method of the creation of diffraction-free beams including the use of optical elements with a strong spherical aberration. Such features as the long beam focal length, the effective suppression of axial intensity oscillations, and the ability to form the beam with the given number of rings and the cone angle are the significant advantages of diffraction-free beams formed using optical elements with a strong spherical aberration over traditional Bessel beams formed by the axicons.

2.1 Investigation of two-element scheme axicon–lens with the high numerical aperture: experimental setup and results

The scheme of an experimental set-up is shown in Fig. 2. Gaussian beam from the He-Ne laser 1 (λ= 0.63 μm) is expanded by the collimator 2 up to the diameter of 2 cm. The linear axicon 3 has the apex angle α = 186 deg. The thick plane-convex high-NA-lens 4, having the form of a half-ball with curvature radius 9.5 mm and refractive index 1.5, is placed behind the axicon in the area of the existence of the Bessel beam. CCD-matrix 6 serves for the registration of 2D structure of the output field.

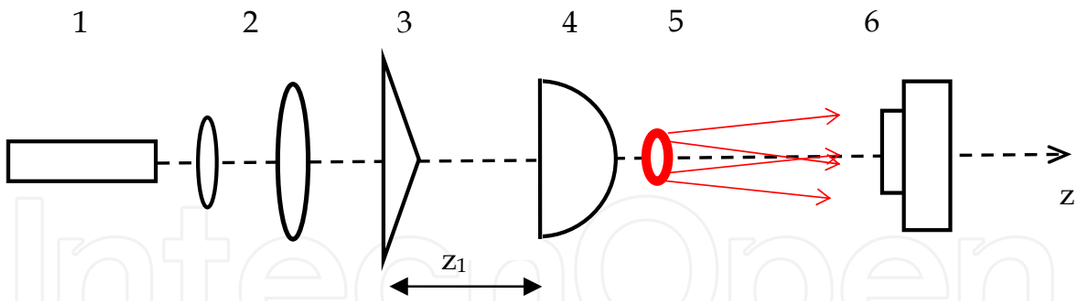

Fig. 2. Experimental setup for the generation of the Bessel-like beam light beam: 1– He-Ne laser; 2–the collimator; 3– the axicon; 4 – the lens with strong spherical aberration; 5 – the annular field in a focal plane; 6– CCD – matrix.

The high-NA-lens 4 focused the Bessel beam into the extended annular field by the external diameter in 0.9 mm. Such annular field serves as a source of a Bessel-like beam generation with the z-dependent cone angle. Fig. 3 demonstrates the transformation of the extended annular field into the Bessel-like beam with z-dependent cone angle γ for different distances z along the focal region of the high-NA-lens (the paraxial focal distance of high-NA-lens is f=1.9 cm). The ratio of external diameter to internal one for annular field is r=2.25 at the starting scanning position in z=1.5cm (Fig. 3, a). The ratio r decreases to 1.2 with the growth of z (Fig. 3, c) and at the distance z=2.3 cm the annular field transforms into the light cloud with the spiral-like structure (Fig. 3, d).

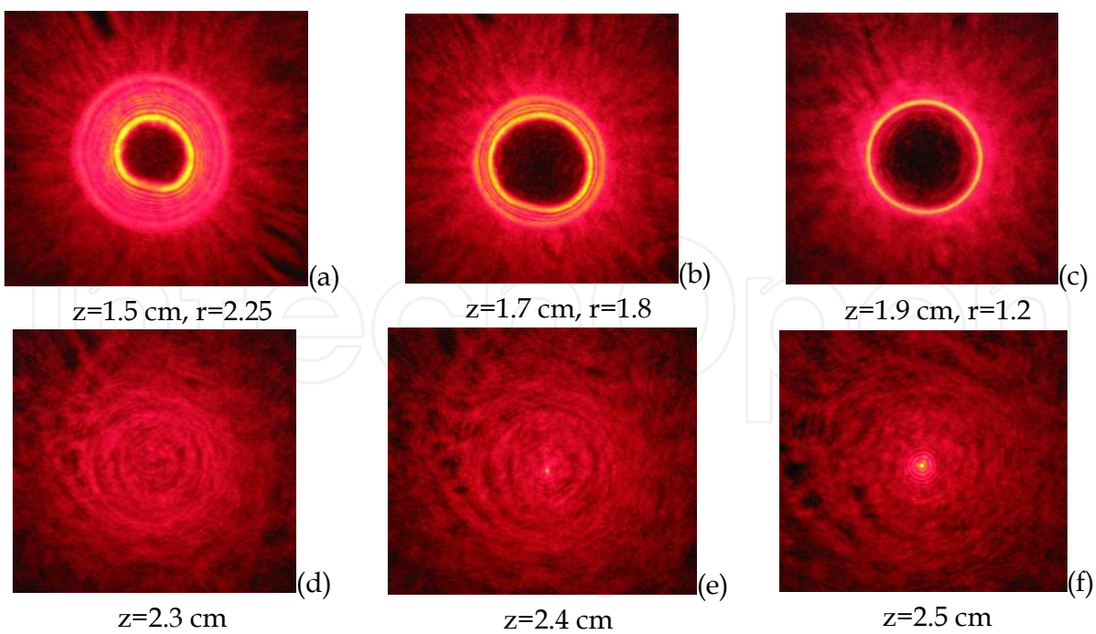

Fig. 3. Evolution of the Bessel-like beam from the extended annular field in two element scheme axicon–high NA-lens, z_1=10 cm.

Origination of the Bessel-like beam with the z-dependent cone angle was captured in Figs. 3, e, d. During the evolution of the Bessel-like beam the external diameter of the annular field remains constant (0.9 mm), but the diapason of variation in the internal diameter is changing from 0.4 mm to 0.8 mm.

The results of measurement of the output beam intensity on the distance z_1 between the axicon and the lens, when a motion of the lens along the optical axis occurs are shown in Figs. 4; 5.

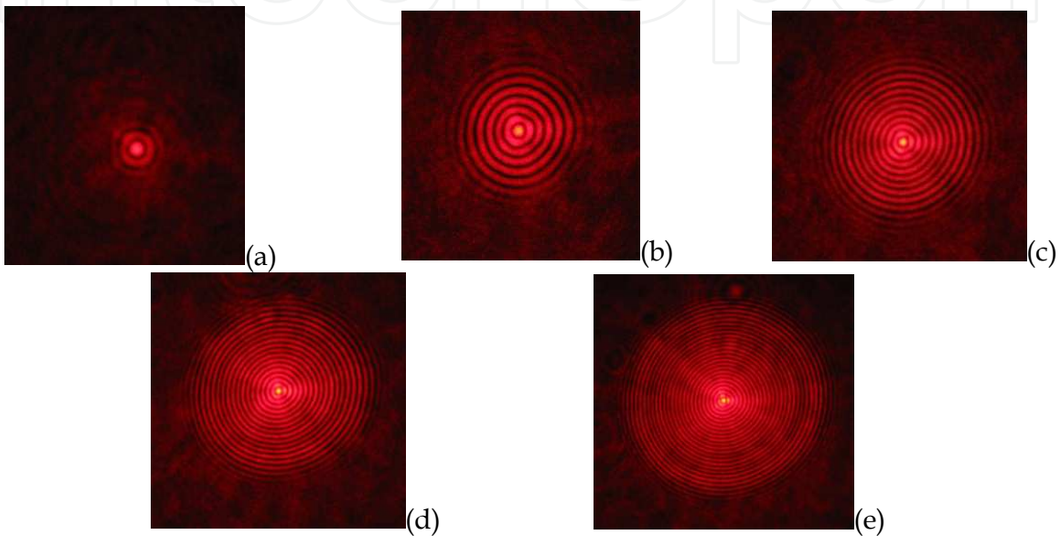

Fig. 4. Photos of the transverse section of the beam at the distance of z_1= 3.5 cm (a); 5.5 cm (b); 6.5 cm (c); 9.5 cm (d); 11.5 cm (e). The distance between the axicon and the CCD-matrix is equal to 64cmhotos of the transverse section of the beam at the distance of z_1= 3.5 cm (a); 5.5 cm (b); 6.5 cm (c); 9.5 cm (d); 11.5 cm (e). The distance between the axicon and the CCD-matrix is equal to 64cm.

On condition of small z_1 the central part of the field is seen to obtain the Bessel-like structure with a small number of rings (Fig. 4, a). With the growth of z_1 the number of rings N increases (Figs. 4; 5, a). A small change of z_1 leads to the essential increase of N and the diameter of the beam (Figs. 4; 5, b). Moreover the boundary between annular field and background is not sharp, but smoothed. It should be noted the growth of the diameter depends linearly on z_1, but the number of rings depends nonlinearly. As a result, the average cone angle of the beam increases, however the speed of this growth decreases (Fig. 5, c). It is an interesting fact that the axial intensity increases with the growth of the number of beam rings (with increasing of z_1) inside the half–focal length of the Bessel beam (after the axicon the focal length of the Bessel beam is ~32 cm) (Fig. 5, d).

Fig. 6 shows the dependence of the diameter of the annular maximum with the serial number N=10 on the distance z. The diameter is seen to increase linearly with z therefore the cone angle changes inversely to z.

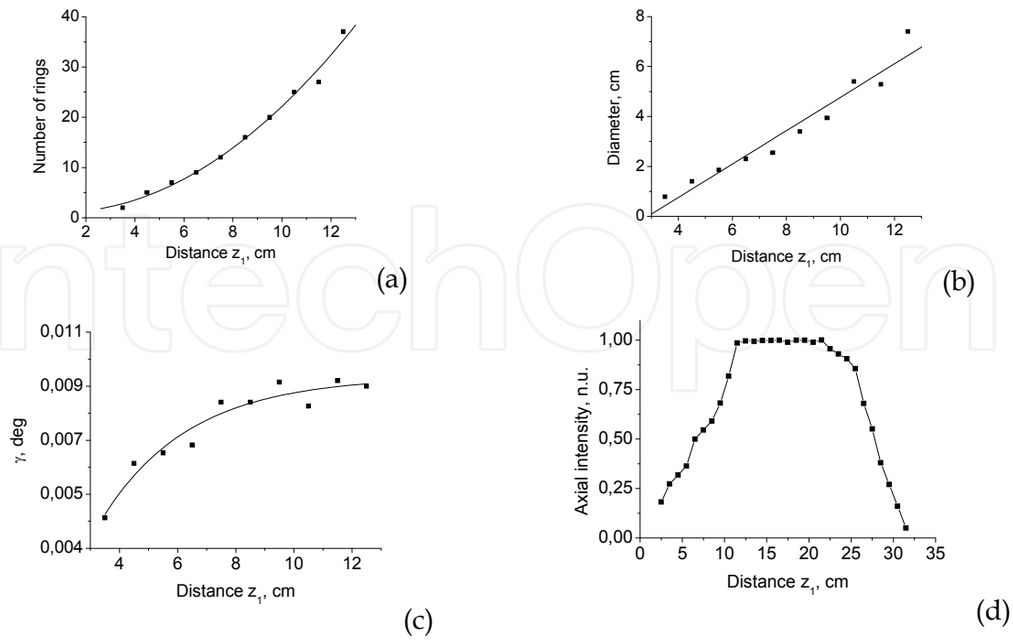

Fig. 5. Dependence on the distance of the number of rings N (a), the diameter of the beam (b), the average cone angle γ (c) and the on-axis intensity (d). Note that in the process of measurements the distance between the axicon and CCD-matrix is unaltered.

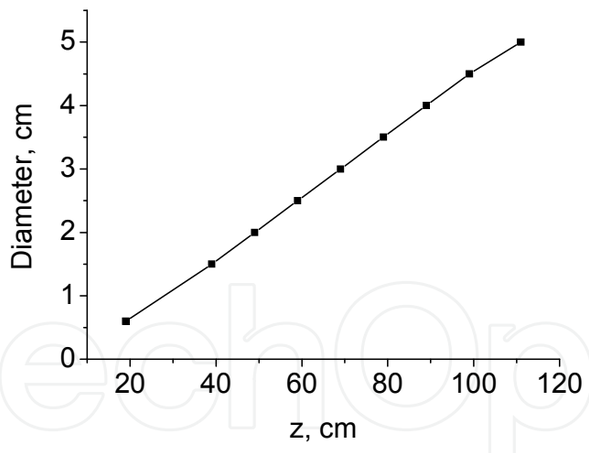

Fig. 6. Change in the Bessel-like beam size D along the longitudinal coordinate z (number of rings N = 10).

2.2 Analysis using Huygens–Fresnel diffraction integral

A quantitative calculation of the scheme with the high-NA lens needs in the application of the vector theory of diffraction. Within the framework of this chapter we will limit ourselves by a scalar approximation (Jaroszewicz & Morales, 1998). Output field amplitude a(ρ, z) for the system of thin lens–axicon–high-NA-lens (Fig. 7) describes by the formula:

$$a(\rho,z)=-\frac{k^2}{z z_1}\int \exp\left[-\frac{\rho_2^2}{w^2(z_0)}+ik\frac{\rho_2^2}{2R(z_0)}-ik\gamma\rho_2+ik\frac{\rho_2^2+\rho_1^2}{2z_1}\right]J_0\left(\frac{k\rho_2\rho_1}{z_1}\right)\rho_2\,d\rho_2\times$$

$$\int \exp\left[-ik\frac{\rho_1^2}{2f^2}-ik\beta\rho_1^4-ik\gamma\rho_2-ik\frac{\rho^2+\rho_1^2}{2z}\right]J_0\left(\frac{k\rho\rho_1}{z_1}\right)\rho_2\,d\rho_2 \qquad (1)$$

where k is a wave number, ρ, ρ_1, ρ_2 are radial coordinates for planes R, L2, A (Fig. 7), $w(z_0) = w_0[1+\lambda^2 z_0^2/\pi^2 w_0^4]$ is the radius of area of the focused Gaussian beam as the function on the longitudinal coordinate z_0, w_0 is a minimal radius of beam, J_0 is the Bessel function of zero order (m=0), f_2 is the focal length of the high-NA-lens L2, $R(z_0)$ is a radius of wave front curvature for the Gaussian beam at the axicon, λ is a wavelength, γ is the cone angle of the axicon, β is an aberrant coefficient for the lens L2.

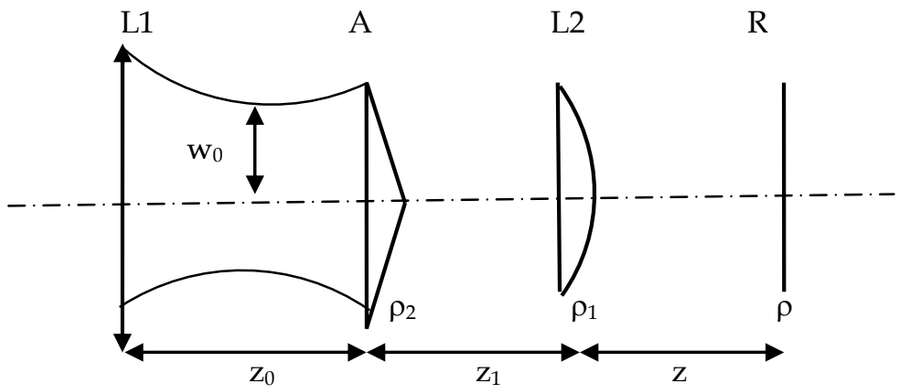

Fig. 7. Optical scheme for the evaluation of diffraction integral.

Results of the calculation for the output field are shown in Fig. 8. The calculation was made for the case when distance between the axicon and the output plane preserves unchangeable (equal to 64 cm), but the distance z_1 between the axicon and the lens changes. It is seen that a strong dependence of the structure of field on z_1 takes place due to spherical aberrations. In the case when z_1.is lower or equal to the paraxial focal length (1.5 cm), the field is a wide ring with the internal radius tending to zero when z_1.increases (Fig. 8, a, b). Sharp change of the field type from wide ring into the beam with intensive axial maximum and oscillated periphery takes place, when z_1 exceeds a little larger the focal length. Fig.8, c, d shows a small modulation depth of the multi-ring field. With further increase of z_1 the modulation depth increases in near-axial region.

Thus, the model of spherical lens satisfied the description of properties of the generated light beam (for example, the dependence of the ring number on distance z_1). It is necessary to notice that this model is not strict because it does not take into account such effects as the dependence of the transmission coefficient of spherical surface on the incident angle.

The conclusion can be made that two-element optical scheme composed of the axicon and the high-NA-lens allows one to create compact a generator of z-dependent Bessel–like beams, where the ring number can be changed due to the shift of lens along the optical axis.

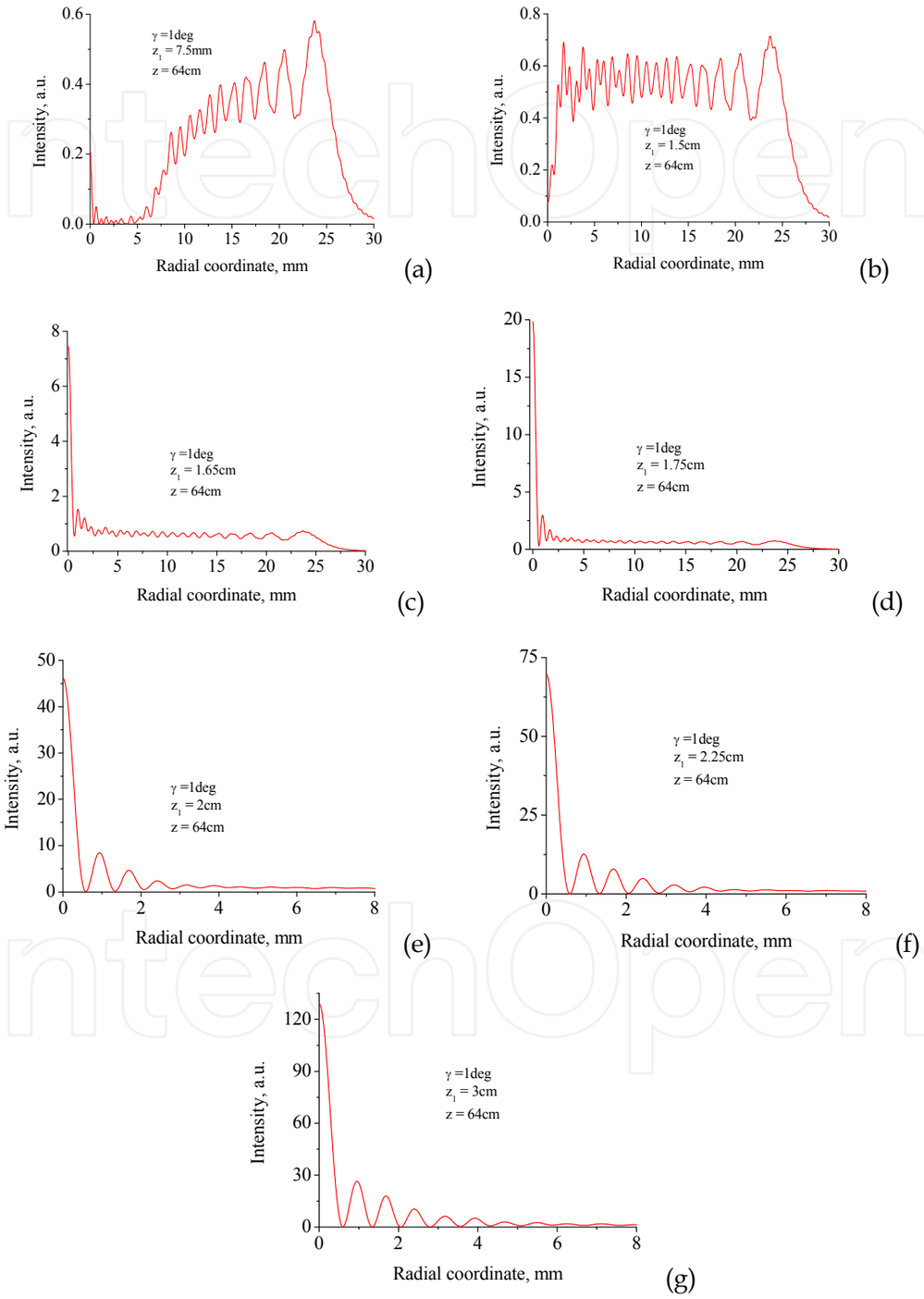

Fig. 8. The influence of the distance between the axicon and the high-NA-lens on the structure of the far- field.

2.3 Scheme with Fourier–transformation of the annular field: formation of the beam with uniform axial intensity and propagation features

The investigation of the far field is the aim of further analysis of the optical scheme with the axicon and the high- NA lens. In the scheme in Fig. 2 the Fourier-transforming lens was used additionally. The front focal plane of this lens was placed in the focal area of high-NA lens (Fig. 9). The focal distance of second lens was equal to 60 cm.

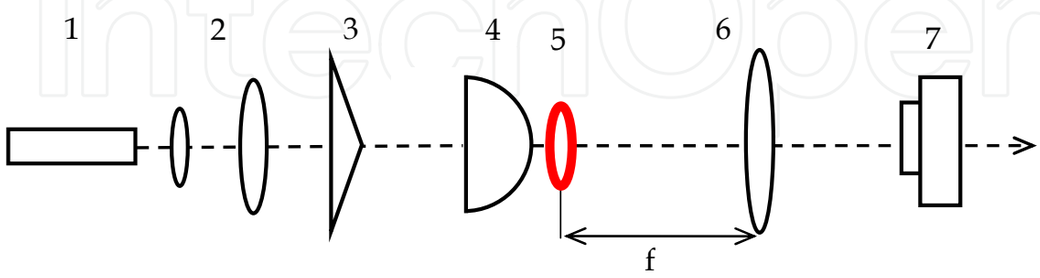

Fig. 9. Experimental setup for the generation of the quasi-Bessel light beam: 1– the He-Ne laser; 2– the collimator; 3– the axicon; 4 – the lens with strong spherical aberration; 5 – the annular field; 6 – the Fourier transforming lens; 7 – CCD – matrix

The field in the back focal plane of the lens and at the further distance had the Bessel type multi–ring structure. This can be easily explained with the use of the thin lens instead of high- NA lens 4. In this case the output field will be a Fourier-transformation of a thin annular beam formed in focal plane after the thin lens. Such a field is known to be the Bessel beam with high accuracy. When the high-NA-lens is used, the thin ring is not formed due to the spherical aberration which influences later on the field in far zone. The Fourier-transformation of the annular field with the large width leads to the formation of some superposition of Bessel beams with different the cone angles and relative phases. The superposition of Bessel beams exhibit new properties, which are not typical for partial Bessel beams. The use of different Bessel beam's superpositions opens the possibility for field synthesis with the given transverse and longitudinal structure. Furthermore, such Bessel–like beam is characterized by a large length of the area, where the axial intensity closes to uniform (within the limit of 13 m the variation of axial intensity amounted to ~ 4% (see Fig. 10)).

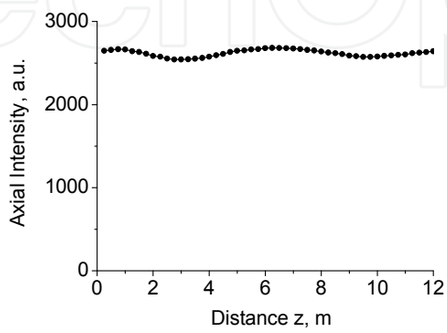

Fig. 10. Axial intensity as a function of longitudinal distance *z* after the Fourier-transforming lens.

This result points out that the annular fields with the large ratio of ring width to average diameter can generate a wideband on angular spectrum Bessel beam with the uniform long-distance focal area.

2.4 Investigation of properties of broadband Bessel–like beams

Two types of objects can be identified among a large variety of light-scattering objects. There are foreign inclusions with distinct boundaries and cloudy media. A matted surface and solutions of suspensions respectively are two-dimensional and three-dimensional analogs of the first type of the medium; a milky scatterer and milky emulsions are analogs of cloudy media. It was shown experimentally (Belyi et al., 2006) that a beam profile reconstruction occurs upon a passage of the Bessel beam through scattering media (solutions of suspensions, emulsions, and matted surfaces). The influence of scattering media on the structure of broadband Bessel–like beams has also been investigated.

Fig. 11 demonstrates the radial distribution of the intensity for the Gaussian beam and broadband Bessel–like beam at their propagation without the matted diffuser (curve 1) and with the matted diffuser (curve 2) along the optical axis of the scheme.

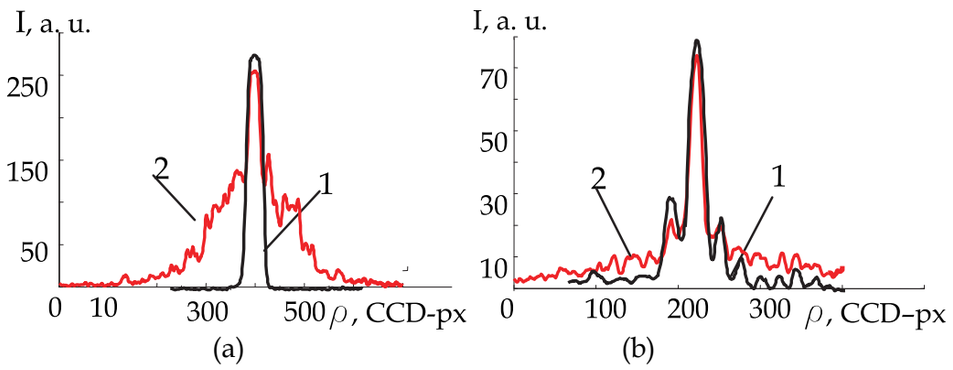

Fig. 11. Radial distribution of intensity: (a) for the Gaussian beam – the curve 1 corresponds to the Gaussian beam profile without the diffuser and the curve 2 is the result of the Gaussian beam passage through the diffuser; (b) the Bessel–like beam – the curve 1 corresponds to the Bessel–like beam profile without the diffuser and the curve 2 is the result of the Bessel–like beam passage through the diffuser

The matted diffuser as the scattering medium was located at the distance of 20 cm after the lens 4 (in the Fig. 2). The width of the Gaussian beam and the width of the central maximum of the Bessel–like beam were chosen out to be approximately identical and about 450–460 μm. The registration plane was located at the distance of 10 cm after the matted diffuser in both of cases. For the Gaussian beam an appearance of a considerable speckle – noise leads to the distortion of the overall picture of the intensity profile. In case of the Bessel–like beam propagation through the light–scattering medium the structure of the central maximum and the rings remain insignificant against speckle–noise (Kramoreva & Rozhko, 2010).

In another case a "regeneration" phenomena of the Bessel–like beam is investigated, when a metal ball with the diameter of 2 mm was chosen as an obstacle for the Bessel–like beam. The ball has been placed at the distance of 34 cm from the high-NA-lens 4 (in the Fig. 2) in

the center of the Bessel–like beam and has overlapped the central and partially the first annular maxima. The registration of the transverse distribution of the intensity has been made at several distances from the ball. In Fig. 12, a, b the 2D distribution of intensity is shown for two distances from the obstacle (lower side of the beam is not shown, i.e. it has been covered by the support for the ball).

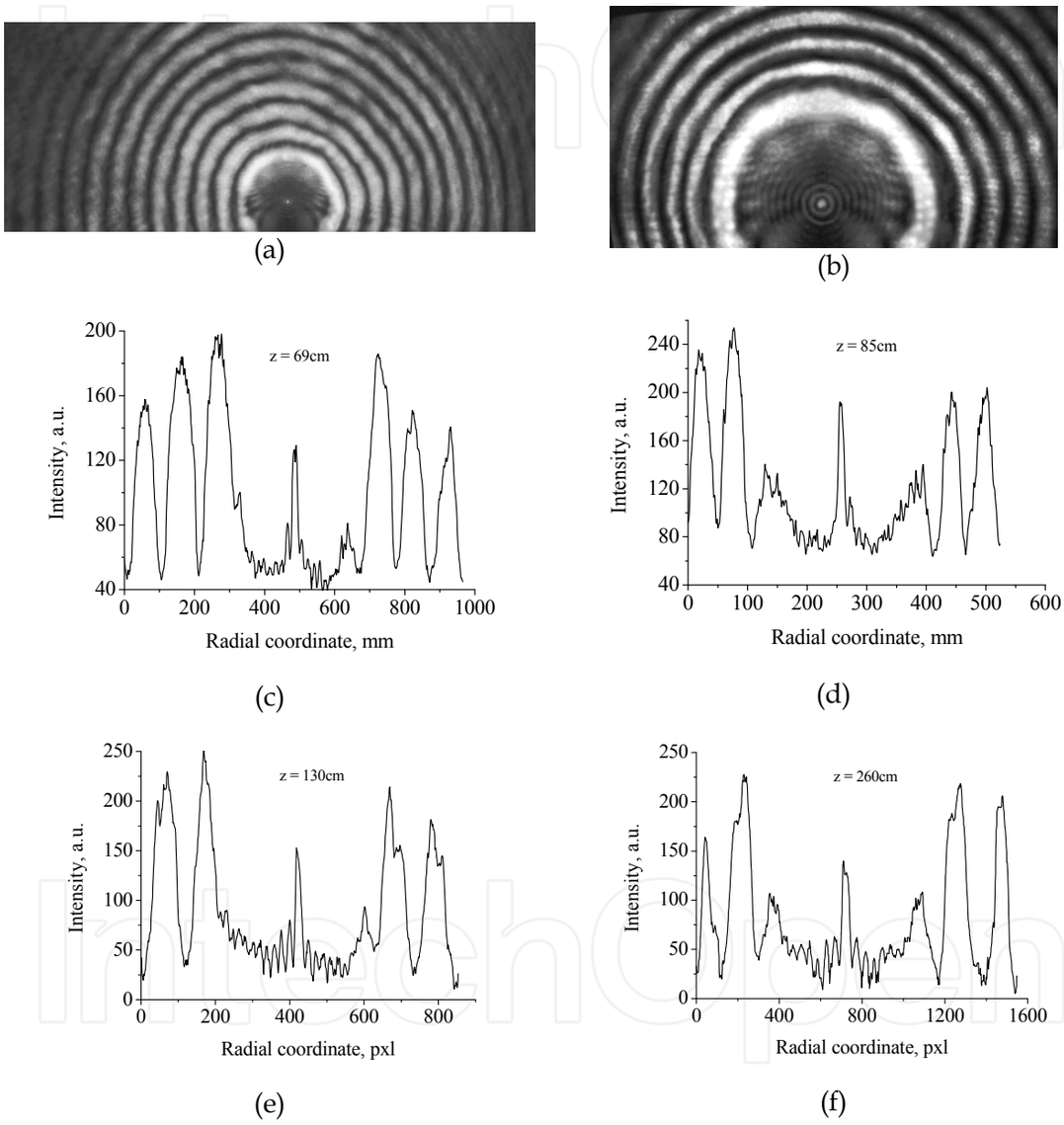

Fig. 12. Photos of transverse intensity distribution of z- dependent Bessel-like beam at distances 69 cm (a) and 260 cm (b) from the ball. 1D intensity distribution of central part of the beam at various distances z (c-f).

Macroscopic dip of the intensity in the center of the beam is the consequence of screening the field by the ball. In the shadow area the multi-ring field which coincides in its sight with Bessel one can be observed. The 1D-cuts of intensity of the shadow field for various z are shown in Fig. 12, c-f.

In this section we present the experimental investigation and the numerical simulation of spatial and angular properties of the light field irradiated by the annular source formed in the scheme composed the axicon and the lens with the strong spherical aberration. The cone angle of such beam decreases smoothly when the beam propagates along the optical axis. The number of rings of the beam depends on the distance between the axicon and the lens. As a result, the pointed scheme is promising for the creation of compact sources of the z-dependent Bessel beam. Using the additional Fourier-transforming lens, the generated field presents itself the Bessel beam with wide angular spectrum. The axial intensity of the beam is characterized by high uniformity at large distance.

The shadow field generated by the beam during the screening of the central zone by the circular obstacle has been investigated. The shadow field is shown to have conical nature, which can be identified on its annular spatial spectrum. The fact that the shadow field appearing at the presence of the obstacle with the ideal edge has azimuthally-symmetrical amplitude-phase distribution is of important practical application. Consequently, the presence of any edge defects will influence on the structure of the shadow field. This opens the possibility to create the method of optical diagnostics of the quality of micro-reliefs. Moreover, the minimal presence of a speckle – noises under the condition of light-scattering is promising for quality improving the tissue structures visualization in the systems of OCT.

In conclusion it is necessary to pay attention to the peculiar type of Bessel light fields, which are formed in conditions of total internal reflection. They are called evanescent light beams. The improved lateral resolution of optical systems using the evanescent Bessel beams as a probe radiation is a rather real possibility.

2.5 Evanescent Bessel beam: theory and simulation analysis

It is known that resolution depends on the diameter of a probing light beam: the less the diameter of the beam, the higher the resolution of the system. Therefore, the growing interest to nonparaxial and evanescent Bessel lights is caused by the availability of submicron structure of the axial maximum, different polarization properties and energy characteristics (Grosjean et al., 2003; Novitsky et al., 2008 as cited in Kurilkina et al., 2010; Rushin & Leizer, 1999; Zhan, 2006).

According to so-called "evanescent field" phenomenon, the appearance of an evanescent field is associated with light internally reflection phenomena when the Gaussian light beam travels from the first optical medium n_1 into the second optical medium with a refraction index n_2 so that $n_2 < n_1$ (for example, for a cornea n_1=1.38 and an aqueous humor n_2=1.336 or for a lens n_1=1.413 and a vitreous humor n_2=1.336). In general an evanescent mode is the wave–guide propagation mode which is known per se and therefore needs not be more specifically described. It is notable that the amplitude of a wave in this mode diminishes rapidly along the direction of its propagation, but the phase does not change. The evanescent Bessel beam has the following features: significantly reduced diameter comparing to the emitted beam; a central lobe is significantly smaller in size than the wavelength of radiation in the medium where the evanescent Bessel beam is generated (a second medium n_2); and a retained tight focus profile along the direction of beam propagation within the desired distance. This desired distance is relatively large for near-field applications (up to several wavelengths), and can be even more increased by using the

third medium interposed between the first and the second media, provided that the refraction index of the second medium is less than the refraction index of each of the first and the third media.

If the propagation direction of circular polarized evanescent Bessel beam is a perpendicular to a boundary of two isotropic media (under a condition of total internal reflection ($n_1 > n_2$)) the representation of transversal component of electric vector for circular polarized evanescent Bessel beam in the optical less dense medium n_2 is (Goncharenko et al., 2001):

$$E_{\perp}^{\pm} = \mp i \sin(\gamma_2)\left[e_{+} J_{m-1}(q\rho)\exp\left(-i(\varphi \mp \alpha)\right) + e_{-} J_{m+1}(q\rho)\exp\left(i(\varphi \mp \alpha)\right)\right]\exp(-\chi z + im\varphi) \quad (2)$$

Here ρ, φ, z are the cylindrical coordinates, $J_m(q\rho)$ is the m-order Bessel function, $k_0 = 2\pi/\lambda$, γ_2 – the cone angle of the Bessel beam in the second medium n_2, $q = \sqrt{(k_0 n_2)^2 + \chi^2}$ - the transversal component of the wave vector, $\sin(\gamma_2)=q/k_0 n_2$, $\tan(\alpha) = \chi / k_0 n_2$, $k_z = i\chi$ is z-projection of the wave vector, $e_{\pm} = (e_1 \pm i e_2)/\sqrt{2}$ are unit circular vectors, e_1, e_2 are unit-vectors of the right (+) and the left (–) circular polarization. In common case, according to Eq. 2 the evanescent Bessel beam is a superposition of two circular-polarized Bessel beams with a different space structure. If m = 0, the transversal component of the electric vector is:

$$E_{\perp}^{\pm} = \mp\sqrt{2}\sin(\gamma_2) J_1(q\rho)[e_1 \sin(\varphi - \alpha) - e_2 \cos(\varphi - \alpha)]\exp(-\chi z) \quad (3)$$

As seen from Eq. 3 in the optical less dense medium n_2 the polarization of the evanescent Bessel beam m=0 becomes linear one.

Azimuthal, radial and z– components of an energy flow of the evanescent Bessel beam are (Goncharenko et al., 2001):

$$S_{\rho} = \frac{4\chi q^3}{k_0^4}\frac{m}{q\rho} J_m^2(q\rho)\exp(-2\chi z), \quad S_{\varphi} = \frac{2(\varepsilon_1 + \varepsilon_2)k_0}{n_1 q}\frac{m}{q\rho} J_m^2(q\rho)\exp(-2\chi z) \quad (4)$$

$$S_z = \left[J_{m-1}^2(q\rho) - J_{m+1}^2(q\rho)\right]\exp(-2\chi z),$$

where $n_{1,2} = \sqrt{\varepsilon_{1,2}}$.

According to Eq. 4 for the evanescent Bessel beam m=0 only the longitudinal z-component of the energy flow occurs in an energy balance, for the evanescent Bessel beam of high order all three components of energy flow are nonzero one.

The important feature of the evanescent Bessel beam is the ability of a spatial localization of its energy. For n_1=2.3, γ_1=40 deg., the diameter of the central lobe for the beam within the range of a evanescent field existence is: $d(\gamma) \approx 4.8\frac{\lambda}{2\pi n_1 \sin(\gamma_1)} \approx 0.5\lambda$.

The penetration depth of the beam inside the medium depends on the cone angle of the evanescent Bessel beam. The growth in the cone angle leads to the penetration depth

decrease as an exponential damping (Fig. 13, a). Fig. 13, b demonstrates a "virtual" jump of energy of the beam into the optically less dense medium.

So, the theoretical analysis demonstrates the ability of the evanescent Bessel beam to realize the localization of light field in a subwavelength space region; the evanescent Bessel beam has a significantly reduced diameter and small number of rings in comparison to initial Bessel beam. The narrow central maximum of evanescent Bessel beam is a nondiffractive one within the range of the evanescent field's existence in comparison to the evanescent Gaussian field. According to the given consideration the evanescent Bessel beam has a promising perspective for application in optical near–field microscopy and OCT.

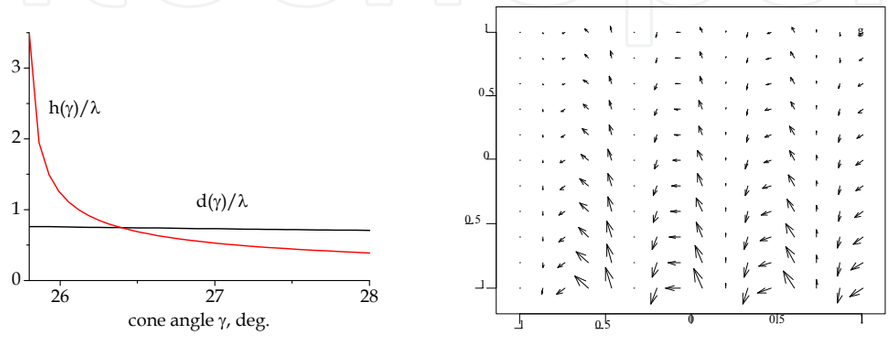

(a) (b)

Fig. 13. Evanescent Bessel beam behavior: the dependence of the penetration depth *h* and the central lobe diameter *d* on the cone angle γ (a); a vector field of the evanescent beam (b).

3. Influence of absorption and optical activity on spatial properties of the quasi-nondiffractive beam

For the optimization of probing condition by the quasi-nondiffractive beam availability of absorption and optical activity in tissues are to be taken into account.

Several publications concern the analysis of nondiffracting beams interaction with an optically active or absorbing medium. The displaying properties of the Bessel beams behavior at their propagation in an optically active media is investigated to a greater extent than for the absorbing media. So, the analysis of Bessel beam behavior propagation along one of the optical axes in biaxial crystals is presented by Kazak et al., 1999. Berry & Jeffray, 2006 have analyzed the image of a conical refraction in terms of singular optics focusing their attention on the fact that the Bessel vortex beams in biaxial crystals are the beams with eigen polarization. Fadeeva & Volyar, 2010 revealed the abnormal zone, where a diffraction-free beam can propagates through a purely chiral crystal as if they do in an isotropic medium. According to the proposed theory even a purely chiral crystal without linear birefringence can generates optical vortices in an initially vortex-free Bessel beam. Spatial features and the polarization pattern of non-paraxial Bessel beams were investigated by Petrova, 2000 in natural optically active media. It is shown that the value of the Bessel beam cone angle influences on the behavior of specific plane-of-polarization rotation.

The problems of Bessel beam interaction with the absorbing media are investigated in a modest way. As regard the interaction of the Bessel beam with the absorbing medium,

Zamboni-Rached, 2006 has developed a method for the simulation of longitudinal intensity pattern of propagating beams in absorbing media. As a particular case, the diffraction-attenuation resistant beams were obtained so that the beams are capable of maintaining both, the size and the intensity of their central spots for long distances compared to ordinary beams. The referred method for absorbing media was developed from appropriate superposition of ideal zero-order Bessel beams. Such beams maintain their resistance to diffraction and absorption even when they are generated by the finite apertures (Zamboni-Rached et al, 2010). At present the behavior of energy flows under a condition of the Bessel beam interaction with absorbing media is studied poorly. However the knowledge about a distribution of energy flows are important to understand the subtle effect of energy swapping inside the beam. Under a condition of interaction of the Bessel beam with the absorbing cylinder a problem is solved partially by Khilo et al., 2005. An analysis of TE- and TH-polarized input field both, the reflection and energy coefficients allows one to evaluate the laser energy loss in an absorbing cylinder and the heat distribution in the cross section.

In this section some features of the interaction of the Bessel beam with a semi-infinite media with absorption and optical activity are presented.

3.1 Bessel beam and absorbing medium: theory and simulation analysis

When incident Bessel beam passes from the transparent isotropic medium with the refraction index n_0 into the semi-infinite isotropic absorption medium n, the refractive index $n = n' + i\,n''$ and the longitudinal component of wave vector $\tilde{k}_z = k_{z1} + i\,k_{z2}$ are complex values. Solutions of Maxwell's equations for TE-, TH-polarized Bessel beam within absorption medium are (Khilo et al., 2005; Petrova & Kramoreva, 2010):

$$E_\rho^{TH} = -\frac{i\tilde{k}_z}{2}\left(J_{m+1}(q\rho) - J_{m-1}(q\rho)\right), \quad E_\varphi^{TH} = -\frac{\tilde{k}_z}{2}\left(J_{m+1}(q\rho) + J_{m-1}(q\rho)\right),$$
$$E_z^{TH} = qJ_m(q\rho)$$
$$E_\rho^{TE} = \frac{ik_0}{2}\left(J_{m+1}(q\rho) + J_{m-1}(q\rho)\right), \quad E_\varphi^{TE} = \frac{k_0}{2}\left(J_{m+1}(q\rho) - J_{m-1}(q\rho)\right), \tag{5}$$
$$E_z^{TE} = 0.$$

Where q is a radial wave number, $q = k_0 n \sin(\gamma)$, γ is the cone angle of the Bessel beam in an absorbing medium. All amplitudes in Eq. 5 involve a common phase factor $\exp[i\tilde{k}_z z + im\varphi]$. For TH- polarized Bessel beam longitudinal (z), radial (ρ), and azimuth (φ) components of Pointing vector and heat flow are

$$S_z = \frac{c}{8\pi} k_0 \left(k'_z\varepsilon' + k''_z\varepsilon''\right)\left\{J_{m-1}^2(q\rho) + J_{m+1}^2(q\rho)\right\}\exp[-2k''_z z]$$

$$S_\rho = \frac{c}{8\pi} k_0\, q\varepsilon'' J_m(q\rho)\left\{J_{m-1}(q\rho) - J_{m+1}(q\rho)\right\}\exp[-2k''_z z] \tag{6}$$

$$S_{\varphi} = \frac{c}{8\pi} k_0 \varepsilon' \frac{m}{\rho} J_m^2(q\rho) \exp\left[-2k_z'' z\right]$$

$$Q(q\rho) = \frac{\omega}{4\pi} \varepsilon'(\omega) \left| E(q\rho) \right|^2 \exp\left[-2k_z'' z\right], \tag{7}$$

where $E(q\rho)E^*(q\rho) = |k|^2 \left(J_{m-1}^2(q\rho) + J_{m+1}^2(q\rho) \right) + 2q^2 J_m^2(q\rho)$

Eqs. 6, 7 and Fig. 14 show that the radial energy flow of the Bessel beam and the availability of heat evolution/absorption areas inside the beam cross–section occur due to absorption.

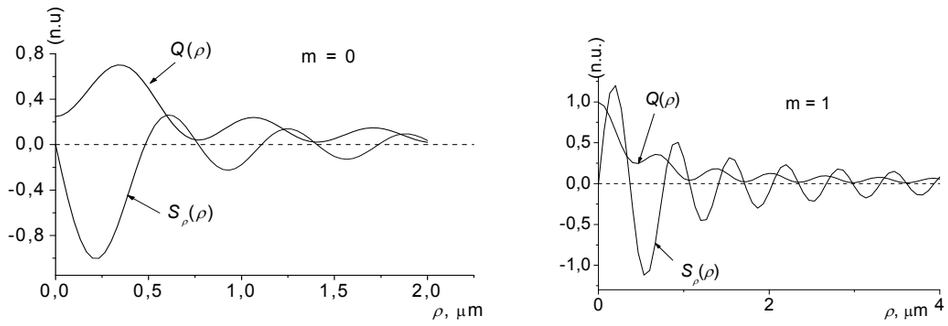

(a) (b)

Fig. 14. Dependence of the radial energy flow and heat flow on the radial coordinate for the Bessel beam with m = 0 (a) and m=1 (b).

Here zero–values of radial energy flow coincide with the minimum or maximum of the heat evolution area in the cross section of the Bessel beam. This property can be useful for the thermal action on tissues in therapeutic area. The heat evolution is a maximal in the region of minimal radial energy flow values. The propagation direction of the radial energy flow S_ρ depends on the order of the Bessel beam. For the Bessel beam with an order m=0 the radial energy flow is directed to the beam axis (Fig.15, a). When we deal with the high order (m=1) Bessel beam, the azimuthal component of energy flow appears and the radial energy flow moves away from the beam axis (Fig. 15, a).

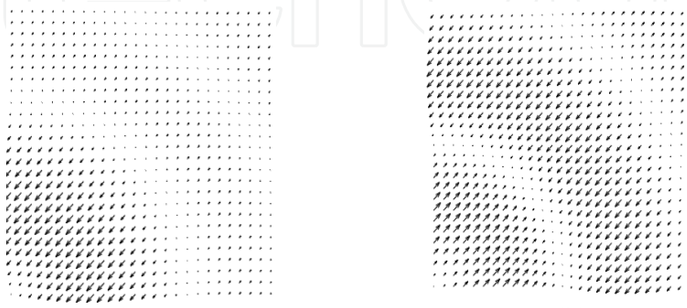

(a) (b)

Fig. 15. Vector field of the radial energy flow for the Bessel beam of different order: m=0 (a), m=1 (b).

Another feature of the beam behavior is that the initiation of azimuthal component of energy flows only for the high-order Bessel beam propagating through an absorbing medium. The change in the azimuthal and radial energy flow direction occurs for different higher m-order of the Bessel function. Fig. 16 shows the oscillation phase shifts in $\pi/2$ and the extension of near-axis minimum with the growth in m. Numerical simulations demonstrate the growth of oscillation frequency in the energy flow under the condition when the cone angle increases (Fig. 17).

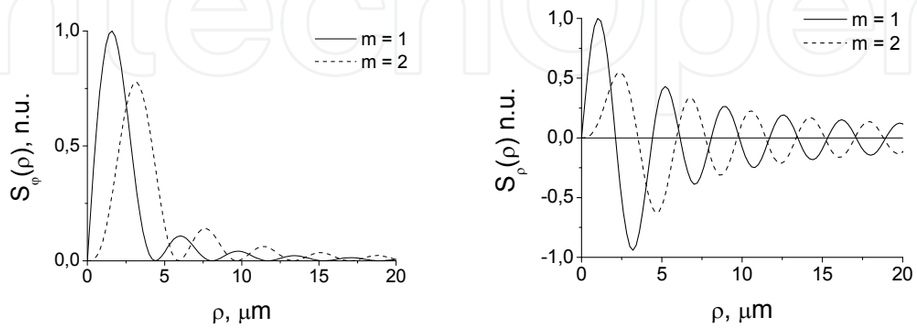

Fig. 16. Energy flow against m –order Bessel beam in an absorbing medium.

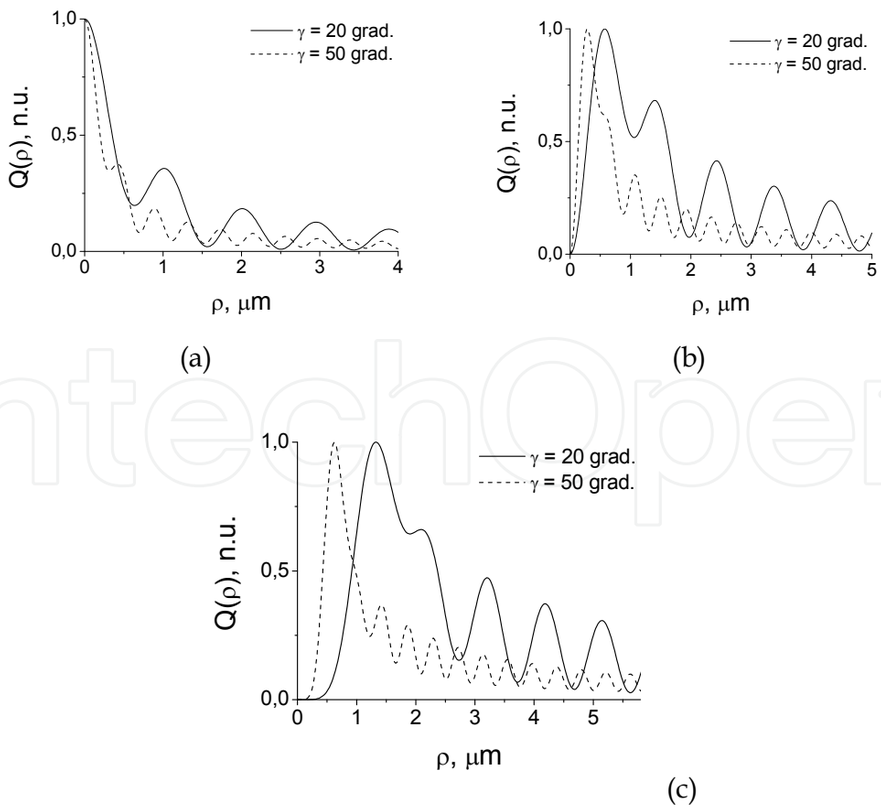

Fig. 17. Cone angle influence on the behavior of heat flow for m = 1 (a); m = 2 (b); m = 4 (c).

In this case the smoothing of Q(ρ) oscillations is the feature for the given function and it is the effect of radial flow contribution in the energy balance of the Bessel beam.

3.2 Bessel beam and optically active medium: theoretical analysis

When TH-polarized Bessel beam travels from the non-absorbing medium n_1 to semi-infinite optically active medium the boundary condition describes by the expression:

$$E_{\tau i}^{TH} + E_{\tau r}^{TH} + E_{\tau r}^{TE} = E_{\tau t}, \quad H_{\tau i}^{TH} + H_{\tau r}^{TH} + H_{\tau r}^{TE} = H_{\tau t}, \tag{8}$$

This formula describes the normal incidence of the beam to the boundary of mediums.

In an optically active medium the refracted field is a circular-polarized Bessel beam with transverse and longitudinal components (Petrova, 2000):

$$\begin{gathered} E_{\rho}^{\pm} = \pm i\left(\frac{m}{q\rho}J_m(q\rho) \pm \cos(\gamma_{\pm})J'_m(q\rho)\right), \\ E_{\varphi}^{\pm} = -\left(\cos(\gamma_{\pm})\frac{m}{q\rho}J_m(q\rho) \pm J'_m(q\rho)\right), \; E_z^{\pm} = \sin(\gamma_{\pm})J_m(q\rho), \\ H_{\rho}^{\pm} = \sqrt{\varepsilon}\left(\frac{m}{q\rho}J_m(q\rho) \pm \cos(\gamma_{\pm})J'_m(q\rho)\right), \\ H_{\varphi}^{\pm} = \pm i\sqrt{\varepsilon}\left(\cos(\gamma_{\pm})\frac{m}{q\rho}J_m(q\rho) \pm J'_m(q\rho)\right), \\ H_z^{\pm} = \mp i\sqrt{\varepsilon}\sin(\gamma_{\pm})J_m(q\rho). \end{gathered} \tag{9}$$

Where $\gamma_{\pm}$ is the cone angle of the Bessel beam in the optically active medium, $\cos(\gamma_{\pm}) = \cos(\gamma_0)[1 \pm (\alpha/\sqrt{\varepsilon})\tan^2(\gamma_0)]$, γ_0 is the cone angle of Bessel beam without taking into account a gyrotropic parameter α.

The relationship between the electric vector E and the magnetic vector B is: $B = \mp i n_{\pm} E$, where $n_{\pm} = \sqrt{\varepsilon} \pm \alpha$. The transverse component of the electric vector for m = 0 is described by formula: $E_{\perp}(q\rho) = -\frac{i\cos(\gamma_{\pm})}{\sqrt{2}}(e_{\rho} + i\tau_{\pm}e_{\varphi})J_1(q\rho)$, where e_{ρ}, e_{φ} are unit-vectors for radial and azimuthal directions, $\tau_{\pm} = 1/\cos(\gamma_{\pm})$ is an ellipticity parameter. In paraxial approximation for the circular polarized Bessel beam the transverse component of electric vector is: $E_{\perp}(q\rho) - i[(e_1 \pm ie_2)/2]J_1(q\rho)\exp(\mp i\varphi)$, where e_1, e_2 are unit-vectors of the right (+) and the left (–) circular polarization.

In this case, coefficients of reflection r_{TH}^{TH}, r_{TE}^{TH} and refraction $t_{\pm}^{TH}$ (±) are

$$r_{TH}^{TH} = \frac{\sqrt{\varepsilon_2}\cos(\gamma_i) - n_1\cos(\gamma_0)}{\sqrt{\varepsilon_2}\cos(\gamma_i) + n_1\cos(\gamma_0)},$$

$$r_{TE}^{TH} = \frac{2\alpha n_1\cos(\gamma_i)\cos(\gamma_0)\tan^2(\gamma_0)}{(n_1\cos(\gamma_0) + \sqrt{\varepsilon_2}\cos(\gamma_i))(n_1\cos(\gamma_i) + \sqrt{\varepsilon_2}\cos(\gamma_0))}, \quad (10)$$

$$t_{\pm}^{TH} = \frac{n_1\cos(\gamma_i)(n_1\cos(\gamma_i) + \sqrt{\varepsilon_2}\cos(\gamma_{\mp}))}{(n_1\cos(\gamma_0) + \sqrt{\varepsilon_2}\cos(\gamma_i))(n_1\cos(\gamma_i) + \sqrt{\varepsilon_2}\cos(\gamma_0))}.$$

The upper index denotes the incident TH-polarized Bessel beam, the lower index – the reflected TH- or TE-polarized beam and also the refracted (±) circular-polarized beam. Therefore, the reflected field contains two mutually orthogonal polarized modes. The gyrotropic parameter α can be found by the measurement of the reflected field intensity.

According to Eq. 10 (±) circular-polarized Bessel beams propagate in an optically active medium with different phase velocities and refractive coefficients. The transversal component of electric field $E_{\perp}^{TH}$ with using of a rotation matrix $\hat{U}(\beta z)$ can be represents as following expression:

$$E_{\perp}^{TH}(\alpha) = t^{(1)}\left[-\frac{m}{q\rho}J_m(q\rho)\cos(\gamma_2)\hat{U}(\varphi_1(z)\begin{pmatrix}0\\1\end{pmatrix} + iJ'_m(q\rho)\cos(\gamma_2)\hat{U}(\varphi_1(z)\begin{pmatrix}1\\0\end{pmatrix}\right] - \\ -\alpha C_1\left[i\frac{m}{q\rho}J_m(q\rho)\begin{pmatrix}1 & 0\\0 & -C_2\end{pmatrix}\hat{U}(\beta z)\begin{pmatrix}1\\0\end{pmatrix} + J'_m(q\rho)\begin{pmatrix}C_2 & 0\\0 & -1\end{pmatrix}\hat{U}(\beta z)\begin{pmatrix}0\\1\end{pmatrix}\right], \quad (11)$$

where:

$$C_1 = \frac{2\,n_1\cos(\gamma_i)\cos(\gamma_0)\tan^2(\gamma_0)}{(n_1\cos(\gamma_0) + \sqrt{\varepsilon_2}\cos(\gamma_i))(n_1\cos(\gamma_i) + \sqrt{\varepsilon_2}\cos(\gamma_0))}, \qquad C_2 = \frac{n_1\cos(\gamma_i)}{\sqrt{\varepsilon_2}},$$

$\beta = k_0\alpha/\cos(\gamma_0)$ is the specific plane-of-polarization rotation, $\varphi_1(z) = \tan^{-1}\left[\frac{\tan(\beta z)}{\cos(\gamma_0)}\right]$,

$\cos(\gamma_2) = \sqrt{\sin^2(\beta z) + \cos^2(\beta z)\cos^2(\gamma_0)}$, $\hat{U}(\beta z) = \begin{pmatrix}\cos(\beta z) & \sin(\beta z)\\ -\sin(\beta z) & \cos(\beta z)\end{pmatrix}$

$$t^{(1)} = \frac{2n_1\cos(\gamma_i)}{n_1\cos(\gamma_0) + \sqrt{\varepsilon_2}\cos(\gamma_i)}$$

Eq. 11 is the invariant expression to sign reversal as $\cos(\gamma_0) \to -\cos(\gamma_0)$. Practically, it means the invariance of polarization modes to the change in the propagation direction of incident Bessel beam.

For the demonstration of TH→TE transformation phenomena we rewrite Eq. 11 as:

$$E_{\perp} = t_{+}^{(1)}\left[E_{\perp}^{+}\exp(i\beta z) + \tau\, E_{\perp}^{-}\exp(-i\beta z)\right]\exp[i(k_z z + m\varphi] \quad (12)$$

$$\text{where} \quad E_{\perp}^{\pm} = E_{\rho}^{\pm} e_{\rho} + E_{\varphi}^{\pm} e_{\varphi}, \; \tau = t_{-}^{TH} / t_{+}^{TH} .$$

For paraxial approximation, when $\tau \to 1$, therefore

$$E_{\perp} = i\sqrt{2}\, t_{+}^{TH} \exp[ik_z z]\left[\cos(\beta z) E_{\perp i}^{TH} + i \sin(\beta z) E_{\perp i}^{TE}\right]. \tag{13}$$

Here $E_{\perp i}^{TH,TE}$ are transversal components of incident TH-, TE-polarized beam. Output field is the superposition of TH-and TE-Bessel beams and the amplitude ratio for beams depends on distance z in an optically active medium complies with the simple harmonic law. When $\beta z = (2d + 1)\pi/2$, and an integer number $d = 0$, we deal with the converting TH-polarization of the Bessel beam into the beam with TE-polarization. Estimation of an oscillation period is $z = \pi/2\beta \sim 3$mm, when $\alpha = 5 \times 10^{-5}$, and $\lambda = 0.63$ μm.

Thus, the incidence of linear-polarized quasi-nondiffractive light beam on the boundary with semi-infinity optically active media leads to the appearance of two mutually orthogonal linear-polarized modes in the reflected field. The gyrotropic parameter can be found by the measurement of the reflected field intensity for nonparaxial beams.

So, when the paraxial circular-polarized quasi-nondiffractive beam propagates in semi-infinity optical active medium the refracted field is the superposition of TH-and TE-Bessel beams and the amplitude ratio for beams depends on longitudinal distance z in the optically active medium by the simple harmonic law and TH↔TE mode transformation phenomenon occurs for this case.

In common theoretical analysis allows one to recognize clearly the interaction features of the quasi-nondiffractive beam with semi-infinity absorbing and optically active media. However, the representation of bio-tissue as a bi- or multi-layer combination of the studied above media is a necessary condition for more correct simulation and optimization of probing condition by optical scanning systems.

4. Future research

Our further researches concern on a modernization of the interference technique based on axicon optics. The comparative analysis of the OCT images for different types of probe beams is the focus of our investigations.

The use of the axicon optics in the time–domain OCT was first investigated by Ding et al., 2002. Ding et al. reported on the incorporation of an axicon lens into the sample arm of the interferometer. Using the axicon lens with a top angle of 160 degrees, the researchers maintained lateral resolution of 10 mm or better over a focusing depth of at least 6 mm. The focusing spot has the intensity that is approximately constant over a greater depth range than when a conventional lens is used. Recently, using the spectral–domain OCT, Leitgeb et al., 2006 proposed a non-dual path imaging scheme for imaging of biological samples. It is known, that conical lenses are used for shaping of Bessel beam field distribution in a range of the focal length, whereas they create a ring shape in the far field. The authors used the advantage of the ring–shaped intensity distribution generated by the axicon in the far field: when this field is focused into the back focal plane of the microscope objective, the intensity distribution at the sample position after the objective is a Bessel field with an extended focal

range. Leitgeb et al. demonstrated 1.5 μm resolution across a 200 μm depth of focus. Lee & Rolland, 2008 reported on the feasibility of using a custom–made micro–optic axicon to create a Bessel beam for the illumination and imaging of biological samples using the spectral–domain OCT. The effectiveness of implementing axicon micro–optics has been demonstrated by imaging a biological sample of an African frog tadpole at various positions of the axial distance. The Bessel beam images show invariant resolution and signal–to-noise ratio over at least of 4 mm focal range, while the Gaussian beam images are already out of focus at the axial distance of 1 mm.

We project to conduct the investigations on a base of the Twyman–Green interferometer. The basic configuration of such interferometer is illustrated in Fig.18.

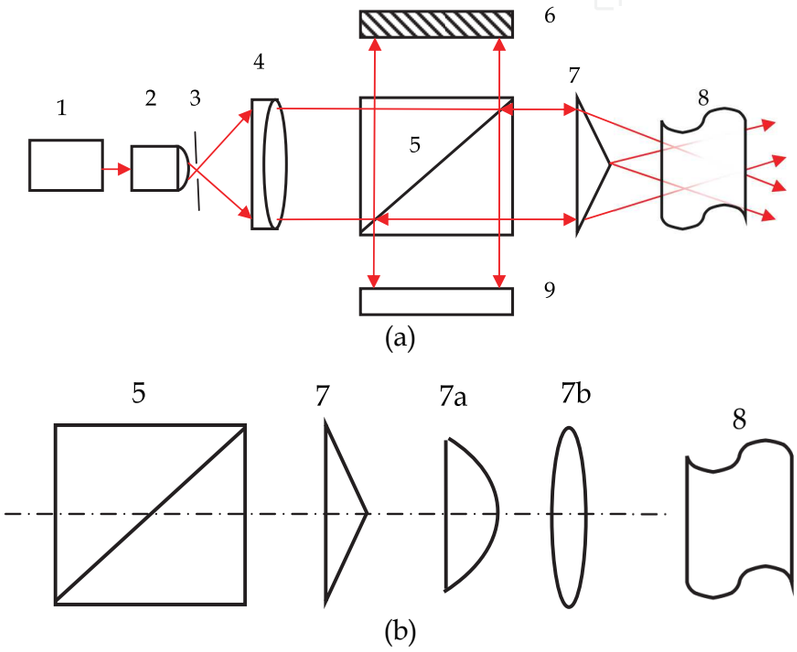

Fig. 18. The optical scheme of the Twyman–Green interferometer with the Bessel beam (a) and the sample arm of the Twyman–Green interferometer with the Bessel – like beam (b):1 – the coherent light, 2 – the microscope objective, 3 – the spatial filter, 4 – the collimator, 5 – the beam splitter, 6 – the reference mirror, 7 – the axicon, 7a – the high NA lens, 7b – the Fourier lens, 8 – the object under test, 9 – CCD. Optical elements 7–7a–7b serves for the generation of the Bessel–like light beam with the uniform axial intensity

The setup consists of a light source 1, a microscope objective 2, a spatial filter 3, a collimator 4, a beam splitter 5, a reference mirror 6, the axicon 7, an object under test 8, and CCD 9.

The light from the source is expanded and collimated by a telescopic system that usually includes the microscope objective 2 and the collimator 4. To obtain a clean wavefront, without diffraction rings on the field the optical components must be as clean as possible. For an even cleaner beam a spatial filter (pinhole) 3 may be used at the focal plane of the microscope objective. The quality of the wavefront that is produced by this telescope, does not need to be extremely high, because its deformations will appear on both interfering wavefronts and not produce any deviations of an interference pattern.

The sample arm of the interferometer involves the axicon for the Bessel beam shaping in the first case (Fig.18, a) and the system of axicon–high NA lens–Fourier lens (7–7a–7b see in Fig.18, b) for the Bessel–like beam shaping with the uniform axial intensity in the second case. The advantage of the given scheme is compactness and a high stability against vibrations.

5. Conclusion

The investigations on improving the quality of OCT-images are currently being pursued in many leading research centers. The methods for solving the problem of improving the axial and lateral resolution of OCT optical schemes and the quality of OCT-images have been resulted from the extensive studies on the optics of Bessel and conical light beams. The idea consists of the necessity to use quasi-nondiffractive Bessel beams and their superpositions as a probe radiation. Such an approach is completely justified owing to the spatial features of Bessel and conical beams, which by their nature are interference fields due to many planar waves. The wave vectors of these waves cover a conical surface causing the formation of a stable interference pattern in the area of the beam focal length. The properties which make Bessel and conical light beams promising in various biomedical sectors are: the suppressed diffraction divergence of the beam pre-axial region, the high lateral resolution in combination with a long focal length, and the reconstruction effect that enables the interaction condition of coherent radiation with an ensemble of microparticles situated in the direction of beam propagation to be significantly smoothed. However, the main drawback of quasi-nondiffractive Bessel beams is the dependence of the axial beam intensity on the axial coordinate. This degrades the energy efficiency of the probe system in various optical systems (in particular, optical tomography systems), which use quasi-nondiffractive Bessel beams.

The development of new methods for forming quasi-diffraction-free beams, including using optical elements with strong spherical aberration, will enable a long focal length of a conical beam and help to achieve the uniform axial intensity.

The theoretical analysis demonstrates the ability of evanescent Bessel beam to localize light field in a sub-wavelength space region. A narrow central maximum of evanescent Bessel beam is a nondiffractive one inside the area of its existence in comparison with the evanescent Gaussian field. In this consideration the use of the evanescent Bessel beam is a promising perspective for improvement of lateral resolution in OCT-system.

New methods of quasi-nondiffractive light beam shaping and the knowledge about the features of interaction of quasi-nondiffractive light beam with different multilayer media allow one to optimize the probing conditions by quasi-nondiffractive light beam. It can be confidently stated that the use of quasi-diffraction-free beams as the probe radiation for increasing simultaneously the lateral and the axial resolution of the OCT optical systems opened a new era for improving the optical tomography.

6. Acknowledgment

Authors would like to thank Vladimir Belyi and Nikolai Khilo (B.I. Stepanov Institute of Physics of the National Academy of Science, Minsk, Belarus) for their support of research, for many productive discussions on the subject and for valuable comments and help during the preparation of this material.

7. References

Andersen, P. E.; Thrane, L.; Yura, H. T.; Tycho, A.; Jorgensen, T. M.; Frosz, M. H. (2004). Advanced modeling of optical coherence tomography systems, *Phys. Med. Biol.*, Vol.49, No. 7, pp. 1307–1327

Arlt, J.; Garces-Chavez, V.; Sibbett, W.; Dholakia, K. (2001). Optical micromanipulation using a Bessel light beam, *Opt. Comm.,* Vol. 197, pp.239-245

Belyi, V.; Kroening, M.; Kazak, N.; Khilo, N.; Mashchenko, A.; Ropot, P. (2005). Bessel beam based optical profilometry, *Proceeding of SPIE 2005 Europe International Symposium Optical Systems Design*, Vol. 5964, pp.59640L1–59640L12, Jena, Germany, Sept. 12–16, 2005

Belyi, V.; Kazak, N.; Khilo, N.; Kramoreva L.; Mashchenko, A.; Ropot, P.; Yushkevich, V. (2006). Influence of scattering media on regular structure and speckle of quasi–nondiffractive Bessel light beams. *Proceeding of SPIE 2006 International Conference Speckle06: Speckles, From Grains to Flowers,* Vol.6341, pp. 6341O-1–6341O-6, Nimes, France, Sept. 13–15, 2006

Berry, M. V.& Jeffray, M.R. (2006). Chiral conical diffraction*, J. Opt. A: Pure Appl. Opt*., Vol.8, pp.363–372

Burval, A. (2004). Axicon imaging by scalar diffraction theory, In: Stockholm. [Electronic resource], 27.07.2009, Available from http:// kth. diva-portal. org/ smash / record. jsf?pid-diva 2:9578

Chauhan, B. C.; McCormick, T. A.; Nicolela, M. T.; LeBlanc, R. P. (2001). Comparison of scanning laser tomography with conventional perimetry and optic disc photography, *Arch. Ophthalmol*., Vol. 119, pp.1492–1499

Ding, Z. H.; Ren, H. W.; Zhao, Y. H.; Nelson, J. S.; Chen, Z. P. (2002). High-resolution optical coherence tomography over a large depth range with an axicon lens, *Opt. Letters*, Vol. 24, No. 4, pp.243–245

Dresel, T.; Schwider, J.; Wehrhahn, A.; Babin, S. (1995). Grazing-incidence interferometry applied to the measurement of cylindrical surfaces, *Opt. Eng*., Vol. 34, pp.3531–3535

Fadeyeva, T. A. & Volyar, A. V. (2010). Nondiffracting vortex-beams in a birefringent chiral crystal, *J. Opt. Soc. Am. A*, Vol. 27, Issue 1, pp. 13–20

Fercher, A. F.; Drexler, W; Hitzenberger, C. K.; Lasser, T. (2003). Optical coherence tomography–principles and applications, *Rep. Prog. Phys.*, Vol. 66, pp. 230–303

Garces-Chavez, V.; McGloin, D.; Melville, H.; Sibbett W.; Dholakia, K. (2002). Simultaneous micromanipulation in multiple planes using a self self-reconstructing light beam, *Nature*, Vol. 419, pp.145–147.

Goncharenko, A. M.; Khilo, N. A.; Petrova, E. S. (2001). Evanescent Bessel light beams, *Proceeding of SPIE 2001 SPIE International Conference Lightmetry: Metrology, Spectroscopy, and Testing Techniques Using Light,* Vol. 4517, pp. 95 – 99, Pultysk, Poland, June 5–8, 2001

Grosjean, T.; Courjon, D; Labeke, D. Van. (2003). Bessel beam as virtual tips for near–field optics*, J. Microscopy*, Vol. 210, pp. 319–323

Jaroszewicz, Z. & Morales, J. (1998). Lens axicon: system composed of a diverging aberrated lens ad a perfect converging lens, *J. Opt. Soc. Am. A*., Vol. 15, No. 9, pp.2383–2390

Kazak, N.; Khilo, N.; Ryzhevich, A. (1999). Generation of Bessel beam under the conditions of internal conical refraction, *Quantum Electronics*, Vol. 29, pp. 1020–1024

Khilo, N. A.; Kramoreva, L. I.; Petrova, E. S. (2005). Reflection and absorption of conical and Bessel light beams by cylindrical objects, *Journal of Applied Spectroscopy*, Vol. 72, No. 5, pp. 663–669

Kramoreva, L. I. & Rozhko, Yu. I. (2010). Optical Coherence Tomography (Review), *Journal of Applied Spectroscopy*, Vol.77, No. 4, pp. 485–506

Kramoreva, L. I. & Rozhko Yu. I. (2010). Visualization of eye structure under the condition of tissue scattering in optical coherence tomography, *Contributed papers 2010 of International Conference Optical Techniques and Nano–Tools for Material and Life Science*, Vol. 2, pp.204–209, ISBN 978–985–6950–31–5, Minsk, Belarus, June 15–19, 2010

Kurilkina, S. N.; Belyi, V. N.; Kazak, N. S.; Al–Saud, Turki S. M.; Al–Khowaiter, Soliman H.; Al–Muhanna, Muhanna. (2010). Application of Evanescent Bessel beams superposition for testing quality of surfaces and thin dielectric layers, *Contributed papers 2010 of International Conference Optical Techniques and Nano–Tools for Material and Life Science*, Vol. 1, pp.38–48, ISBN 978–985–6950–31–5, Minsk, Belarus, June 15–19, 2010

Lee, Kye–Sung & Rolland, J. P. (2008). Bessel beam spectral–domain high–resolution optical coherence tomography with micro–optic axicon providing extended focusing range, *Opt. Letters*, Vol. 33, No. 15, pp.1696–1698

Leitgeh, R. A.; Villiger, M.; Bachmann, A. H.; Steinmann, L.; Lasser, T. (2006) Extended focus depth for Fourier domain optical coherence microscopy, *Opt. Letters*, Vol.31, No. 16, pp.2450–2452

McGloin, D. & Dholakia, K. (2005). Bessel beams: diffraction in a new light, *Contemp. Phys.*, Vol. 46, pp.15-28

Petrova, E. S. (2001). Bessel light beams in gyrotropic medium, *Proceeding of SPIE 2001 International Conference Optics of Crystals,* Vol.4358, pp. 265–271, Mozyr, Belarus, Sept. 26–30, 2006

Petrova E. S. & Kramoreva, L. I. (2010). Features of tissue probing by conic light beams, *Contributed papers 2010 of International Conference Optical Techniques and Nano–Tools for Material and Life Science*, Vol. 2, pp.160–165, ISBN 978–985–6950–31–5, Minsk, Belarus, June 15–19, 2010

Rushin, S. & Leiser, A. (1999). Evanescent Bessel Beam, *J. Opt. Soc. Am. A.*, Vol.15, pp. 1139–1143

Schmitt, J. M. & Knuttel, A. (1993). Measurement of optical-properties of biological tissues by low-coherence reflectometry, *Appl. Opt.*, Vol.32, pp.6032–6042

Turchin, I. V.; Sergeeva, E. A.; Dolin, L. S.; Kamensky, V. A. (2003). Estimation of biotissue scattering properties from OCT images using a small-angle approximation of transport theory, *Laser Phys.*, Vol.13, pp.1524–1529

Zamboni-Rached, M. (2006). Diffraction-Attenuation resistant beams in absorbing media, *Opt. Express*, Vol.14, pp.1804–1809

Zamboni-Rached, M.; Ambrosio, L. A.; Hernandez-Figueroa, H.E. (7Jul 2010). Diffraction-Attenuation Resistant Beams: their Higher Order Versions and Finite-Aperture Generations, In: Arxiv. org., 07.04.2011, Available from http: // arxiv.org/abs/1007.1046v1 [physics.optics]

Zhan, Q. (2006). Evanescent Bessel beam generation via surface plasmon resonance excitation by a radially polarized beam, *Opt. Letters*, Vol.31, pp.1725-1728

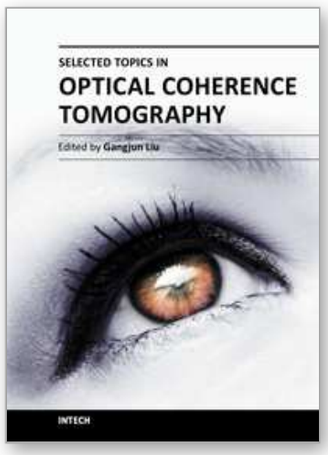

Selected Topics in Optical Coherence Tomography

Edited by Dr. Gangjun Liu

ISBN 978-953-51-0034-8
Hard cover, 280 pages
Publisher InTech
Published online 08, February, 2012
Published in print edition February, 2012

This book includes different exciting topics in the OCT fields, written by experts from all over the world. Technological developments, as well as clinical and industrial applications are covered. Some interesting topics like the ultrahigh resolution OCT, the functional extension of OCT and the full field OCT are reviewed, and the applications of OCT in ophthalmology, cardiology and dentistry are also addressed. I believe that a broad range of readers, such as students, researchers and physicians will benefit from this book.

InTech Europe
University Campus STeP Ri
Slavka Krautzeka 83/A
51000 Rijeka, Croatia
Phone: +385 (51) 770 447
Fax: +385 (51) 686 166
www.intechopen.com

InTech China
Unit 405, Office Block, Hotel Equatorial Shanghai
No.65, Yan An Road (West), Shanghai, 200040, China
中国上海市延安西路65号上海国际贵都大饭店办公楼405单元
Phone: +86-21-62489820
Fax: +86-21-62489821

IntechOpen